Physics of Fluids

LETTER | MAY 12 2023

Squirming with a backward-propelling cage

J. Della-Giustina ; H. Nganguia ; E. Demir

Physics of Fluids 35, 051703 (2023)
https://doi.org/10.1063/5.0152711

Physics of Fluids LETTER pubs.aip.org/aip/pof

Squirming with a backward-propelling cage

Cite as: Phys. Fluids **35**, 051703 (2023); doi: 10.1063/5.0152711
Submitted: 31 March 2023 · Accepted: 28 April 2023 ·
Published Online: 12 May 2023

J. Della-Giustina,[1] H. Nganguia,[1,a)] and E. Demir[2,a)]

AFFILIATIONS

[1]Department of Mathematics, Towson University, Towson, Maryland 21252, USA
[2]Department of Mechanical Engineering and Mechanics, Lehigh University, Bethlehem, Pennsylvania 18105, USA

[a)]Authors to whom correspondence should be addressed: hnganguia@towson.edu and demir@lehigh.edu

ABSTRACT

A squirmer enclosed in a droplet represents a minimal model for some drug delivery systems. In the case of a spherical squirmer swimming with a spherical cage in a Newtonian fluid [Reigh *et al.*, "Swimming with a cage: Low-Reynolds-number locomotion inside a droplet," Soft Matter **13**, 3161 (2017)], it was found that the squirmer and droplet always propelled in the same direction albeit at different speeds. We expand the model to include particles' shape and medium's heterogeneity, two biologically relevant features. Our results reveal a novel behavior: a configuration that consists of a spherical squirmer and a spheroidal droplet in highly heterogeneous media yields a backward motion of the droplet.

The past few decades have seen tremendous progress in modern medicine, especially in the ways drugs and treatments are administered. Targeted drug delivery, a class of methods to deliver medication to specific organs or tissues, shows a great potential for reducing adverse drug reactions. One form of targeted drug delivery consists of inserting the drug in a *carrier*, a micro- or nano-particle,[1–7] that is then absorbed by the patient orally or via an injection. Two features, design and control, must be carefully considered for effective and efficient drug delivery. Design must account for various factors, including but not limited to biocompatibility, capacity, and shape.[8,9] Experimental and numerical studies have shown that under flow conditions and in the presence of red blood cells, non-spherical shapes display better localization toward the blood vessel walls compared to spherical particles. This enhanced localization is particularly important for the carrier's ability to adhere to and ultimately cross biological barriers.[10,11]

On the other hand, the control of a targeted drug delivery system relies on either detectability or predictability of the carrier's motion, the latter of which mimics biological microorganisms.[12] The propulsion of microorganisms in unbounded fluids has attracted tremendous amount of interest since the pioneering works of Taylor[13] and Lighthill.[14] Studies have since extended these seminal works to investigate the propulsion of microorganisms in non-Newtonian and heterogeneous media.[15–23] However, applications including targeted drug delivery,[12,24] or the development of nanotechnologies to manipulate cells,[25] have led to increasing interest in the motion of microorganisms in confined spaces.[25–34]

Theoretical studies of such systems assumed physical interfaces with various properties.[31,35,36] For instance, Reigh *et al.*[31] considered a squirmer inside a clean droplet (surfactant/contaminant-free and Newtonian) and obtained analytical solutions for the squirmer and droplet speeds in a concentric configuration (the squirmer and droplet share the same center). With this configuration, they showed that the squirmer always moves faster than the droplet. Later studies showed that these results also extend to droplet covered with surfactants.[35] These recent findings have provided important insight on locomotion inside a droplet. However, the results are limited to spherical squirmers enclosed in spherical droplets in homogeneous Newtonian fluids.

In reality, microorganisms often encounter heterogeneous environments.[29,37–40] The heterogeneous media can be modeled using the Brinkman equation[41] that accounts for the additional hydrodynamic resistance due to the network of stationary obstacles. It has been employed to probe the effects of viscous heterogeneous environments on locomotion performance.[17,42,43] In terms of shape, several microorganisms can be approximated by spheroids. For example, many ciliates have a mean length-to-width aspect ratio of approximately 2.[44,45] Thus, the spheroidal squirmer[46–49] provides a more biologically accurate model compared to the classical spherical squirmer.[14,50] Moreover, the spheroidal model serves as a first approximation to other non-spherical swimmers (e.g., *E. coli*) to assess how shape affects swimming performance.

The combined effect of fluid heterogeneity and shape is expected to increase the complexity of the squirming motion and the droplet's propulsion; however, the problem has yet to be investigated. Here, we

analyze the influence of these two factors on the propulsion speeds of the squirmer and droplet using numerical simulations. We find nontrivial propulsion speed profiles that depend not only on heterogeneity and shape but also on the viscosity contrast between fluids. Most strikingly, we observe a backward motion of the droplet that results from vortex-like flow patterns moving the droplet in the direction of the surrounding flow, opposite the motion of the squirmer.

We consider the propulsion of a squirmer in a Newtonian pocket enclosed in a drop within a heterogeneous medium, as illustrated in Fig. 1. Following Reigh *et al.*,[31] we assume that the droplet does not deform, for instance as the result of sufficiently large surface tension on its surface. The fluid phases inside and outside the droplet have viscosities μ_1 and μ_2, respectively. We extend the axisymmetric Stokes–Brinkman model presented in our previous study[34] to account for the motion of the droplet. Denoting dimensional variables with a ($\tilde{}$), the region inside the droplet (phase 1 in Fig. 1) is modeled as a purely viscous homogeneous fluid governed by the incompressible Stokes equation $\tilde{\nabla}\tilde{p}_1 + \mu_1\tilde{\nabla}\times(\tilde{\nabla}\times\tilde{\boldsymbol{u}}_1) = \mathbf{0}$, whereas the heterogeneous medium that describes phase 2 is governed by the incompressible Brinkman equation[41] $\tilde{\nabla}\tilde{p}_2 + \mu_2\tilde{\nabla}\times(\tilde{\nabla}\times\tilde{\boldsymbol{u}}_2) + \mu_2\omega^2\tilde{\boldsymbol{u}}_2 = \mathbf{0}$, where ω^{-2} is the permeability of the medium. The governing equations are solved together with boundary conditions in the far-field, $\tilde{\boldsymbol{u}}_2 = \mathbf{0}$, on the squirmer surface, $\tilde{\boldsymbol{u}}_1 = \tilde{\boldsymbol{U}}_S + \tilde{\boldsymbol{u}}_{sq}$, and on the droplet surface, $\tilde{\boldsymbol{u}}_1\cdot\boldsymbol{n} = \tilde{\boldsymbol{u}}_2\cdot\boldsymbol{n} = \tilde{\boldsymbol{U}}_D\cdot\boldsymbol{n}, \tilde{\boldsymbol{u}}_1\cdot\boldsymbol{t} = \tilde{\boldsymbol{u}}_2\cdot\boldsymbol{t}, \mu_1\tilde{\mathbf{T}}_1\cdot\boldsymbol{t} = \mu_2\tilde{\mathbf{T}}_2\cdot\boldsymbol{t}$. $\tilde{\boldsymbol{U}}_S$ and $\tilde{\boldsymbol{U}}_D$ are the squirmer's and droplet's propulsion speeds, respectively, $\boldsymbol{n}$ and $\boldsymbol{t}$ are the normal and tangential vectors on the droplet, the stresses $\tilde{\mathbf{T}}_j = -\tilde{p}_j\mathbf{I} + [\tilde{\nabla}\tilde{\boldsymbol{u}}_j + (\tilde{\nabla}\tilde{\boldsymbol{u}}_j)^T]$ ($j = 1, 2$), and $\tilde{\boldsymbol{u}}_{sq} = \sum_{n=1}^{\infty} B_n V_n \boldsymbol{e}_\zeta$, denotes the tangential velocity on the surface of the squirmer with swimming modes B_n and $V_n = (\tau_0^2 - \zeta^2)^{-1/2} P_n^1(\zeta)$ for a spheroidal squirmer.[46–49] Here, P_n^1 are the associated Legendre polynomials, and the shape parameter $\tau_0 = 1/e_s$, where e_s is the squirmer's eccentricity. The limit $e_s \to 0$ (or $\tau_0 \to \infty$) corresponds to a spherical squirmer, in which case $V_n = -2P_n^1(\zeta)/[n(n+1)]$ and $\zeta \to \cos\theta$.[14,50]

We nondimensionalize the problem as follows: Velocities are scaled by the first mode B_1, and lengths are scaled by the semi major axis of the squirmer a_s. The dimensionless droplet size is denoted by $\chi = a_d/a_s > 1$, where a_d is the semi major axis of the droplet. Finally, stress and pressure are scaled by $\mu_2 B_1/a_s$. In the case of a spherical squirmer in a spherical droplet, a_s and a_d denote the radii of the squirmer and droplet, respectively. In dimensionless form, the Stokes equation in the inner domain becomes

$$\nabla p_1 + \lambda\nabla\times(\nabla\times\boldsymbol{u}_1) = \mathbf{0}, \tag{1}$$

where the viscosity ratio $\lambda = \mu_1/\mu_2$. The dimensionless Brinkman equation in the outer domain is given by

$$\nabla p_2 + \nabla\times(\nabla\times\boldsymbol{u}_2) + \delta^2\boldsymbol{u}_2 = \mathbf{0}, \tag{2}$$

where the fluid resistance $\delta = a_s\omega$. The dimensionless boundary conditions:

$$\boldsymbol{u}_2 = \mathbf{0}, \tag{3}$$

$$\boldsymbol{u}_1 = \boldsymbol{U}_S + \boldsymbol{u}_{sq}, \tag{4}$$

$$\boldsymbol{u}_1\cdot\boldsymbol{n} = \boldsymbol{u}_2\cdot\boldsymbol{n} = \boldsymbol{U}_D\cdot\boldsymbol{n}, \tag{5}$$

$$\boldsymbol{u}_1\cdot\boldsymbol{t} = \boldsymbol{u}_2\cdot\boldsymbol{t}, \tag{6}$$

$$\lambda\mathbf{T}_1\cdot\boldsymbol{t} = \mathbf{T}_2\cdot\boldsymbol{t}, \tag{7}$$

where

$$\boldsymbol{u}_{sq} = \sum_{n=1}^{\infty}\beta_n V_n \boldsymbol{e}_\zeta \tag{8}$$

and the dimensionless swimming modes $\beta_n = B_n/B_1$. While β_{2n+1} modes contribute to propulsion of a spheroidal squirmer,[49] the speeds of a translating spherical micro-organism in an unbounded Newtonian fluid[14,50] and heterogeneous medium[23] depend solely on the first swimming mode. Thus, we only retain β_1 in the surface velocity equation (8). The governing equations are solved numerically using the finite element method implemented in the COMSOL Multiphysics environment. We validate our numerical implementation against the results from Reigh *et al.*,[31] and the analytical solutions using a spherical squirmer and a spherical droplet in a heterogeneous medium. The squirmer and droplet speeds are calculated after applying the force-free condition $\int_S \mathbf{T}_j\cdot\boldsymbol{n}\,\mathrm{d}S = \mathbf{0}$ and are given by

$$\begin{aligned} U_S = \frac{1}{3\mathscr{B}}\{&(\chi-1)^2(3+6\chi+4\chi^2+2\chi^3)\\ &\times(18+18\chi\delta+3\chi^2\delta^2+\chi^3\delta^3)\\ &+6[-9-9\chi\delta+15\chi^2+9\chi^5\\ &+(15\chi^3+9\chi^6)\delta+(\chi^7-\chi^2)\delta^2]\lambda\}, \end{aligned} \tag{9}$$

and

$$U_D = \frac{30\chi^2(1+\chi\delta)\lambda}{\mathscr{B}}, \tag{10}$$

where $\mathscr{B} = (\chi^5-1)(18+18\chi\delta+3\chi^2\delta^2+\chi^3\delta^3) + (2+3\chi^5)(9+9\chi\delta+\chi^2\delta^2)\lambda$. The results in Reigh *et al.*[31] are recovered by taking the limit $\delta\to 0$. The squirmer and droplet speeds become $U_S = 2[3+5\chi^2(\lambda-1)-3\lambda+\chi^5(2+3\lambda)]/[6(\lambda-1)+\chi^5(6+9\lambda)]$ and $U_D = 10\chi^2\lambda/[6(\lambda-1)+\chi^5(6+9\lambda)]$. These equations are identical to those in Reigh *et al.*[31] after letting $\lambda = 1/\tilde{\lambda}$, where $\tilde{\lambda}$ is the viscosity ratio in their work. Figures 2(a) and 2(b) show the propulsion speeds of the squirmer and droplet, while Fig. 2(c) shows the ratio of the droplet to squirmer speeds as a function of the domain size χ with $\delta = 10^{-3}$. The solid curves denote the results using the purely viscous system in Reigh

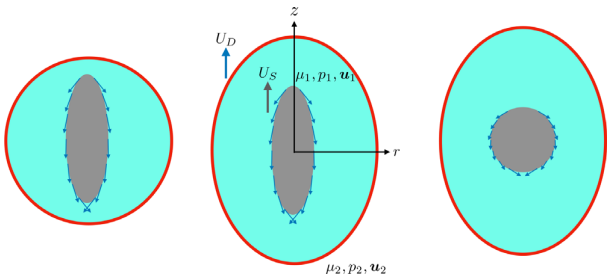

FIG. 1. Schematic of the three squirmer/droplet shape configurations: a spheroidal squirmer in a spherical droplet (left), a spheroidal squirmer in a spheroidal droplet (center), and a spherical squirmer in a spheroidal droplet (right). The squirmer is in a Newtonian fluid pocket with viscosity μ_1 that is enclosed in a droplet in a heterogeneous medium with viscosity μ_2. The squirmer and droplet propel with speeds U_S and U_D, respectively.

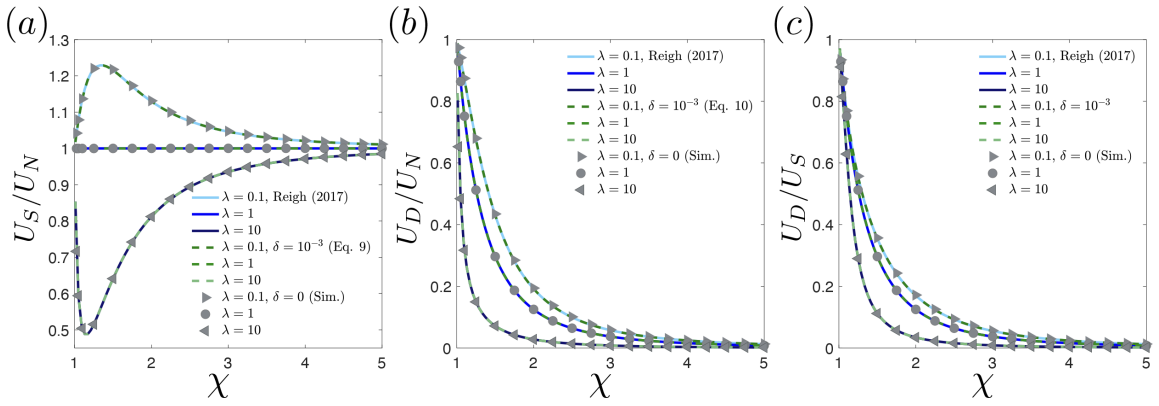

FIG. 2. Propulsion speed for (a) the squirmer and (b) the droplet as a function of the domain size χ. In both panels, the speed is scaled by $U_N = 2/3$, the propulsion speed of a squirmer in an unbounded domain in a Newtonian fluid. (c) Ratio of the droplet to squirmer speeds as a function of the domain size χ. The solid curves denote the results using the purely viscous system [Eqs. (10) and (11) in Reigh *et al.*[31]], the dashed curves are obtained from Eqs. (9) and (10), and the symbols denote numerical simulations. In all panels, the fluid resistance $\delta = 10^{-3}$.

et al.,[31] the dashed curves are obtained from Eqs. (9) and (10), and the symbols denote numerical simulations.

We now analyze the squirmer and droplet speeds for the three configurations shown in Fig. 1: a spheroidal squirmer in a spherical droplet (C_1), a spheroidal squirmer in a spheroidal droplet (C_2), and a spherical squirmer in a spheroidal droplet (C_3). Shapes are characterized by varying the eccentricities of the squirmer e_s and the droplet e_d. In our analyses, the squirmer speed is scaled by the speed U_N of its counterpart in an unbounded Newtonian fluid, where $U_N = 2/3$ for a spherical squirmer or $U_N = \tau_0[\tau_0 - (\tau_0^2 - 1)\coth^{-1}\tau_0]$ for a spheroidal squirmer. To analyze the droplet speed, we scale it by the squirmer speed. The resulting ratio provides a measure of the relative magnitudes of the squirmer and droplet speeds. In all analyses, the droplet size χ varies based on the configuration, whereas we consider squirmer's eccentricities $e_s = 0,\ 0.3,\ 0.9$, droplet's eccentricities $e_d = 0,\ 0.3,\ 0.9$, and the viscosity ratios $\lambda = 0.1, 1, 10$. Finally, while the terms "initial" and "terminal" are often reserved for transient variables, we employed them to denote the speeds in the limits $\delta \to 0$ and $\delta \to \infty$, respectively.

Figure 3 illustrates the propulsion speed of the squirmer U_S normalized by the propulsion speed of a spheroidal (configurations C_1 and C_2) or spherical (configuration C_3) squirmer in an unbounded Newtonian fluid, as a function of the fluid resistance δ. Generally, the dynamics can be split based on the viscosity ratio λ. When $\lambda \leq 1$, the enclosed squirmer always propels slower compared to an unbounded squirmer. Moreover, U_S is non-monotonic as a function of χ: the speed first decreases from χ near 1, reaches a minimum, and then increases to $U_S \to U_N$ as $\chi \to \infty$. For $\lambda \leq 1$ and fixed χ [Figs. 3(a), 3(b), 3(d), 3(e), 3(g), and 3(h)], higher eccentricity yields larger initial speed while the terminal speed depends on the configuration. For C_1, C_2 and fixed χ [Figs. 3(b) and 3(e)], higher eccentricity still yields larger terminal speeds, whereas increasing the eccentricity of the drop e_d in C_3 [Fig. 3(h)] may lead to lower terminal speeds. Note that unlike smaller viscosity ratios, for $\lambda = 1$, the initial speed varies little from U_N when $\delta < 1$.

Propulsion speeds $U_S > U_N$ can be achieved for $\lambda > 1$ and $1 \leq \delta < 10$, as illustrated in Figs. 3(c), 3(f), and 3(i). Compared to the cases $\lambda \leq 1$, the χ-dependent non-monotonic behavior now reaches a maximum speed before converging to U_N as $\chi \to \infty$. Considering the full range of fluid resistance δ, the terminal speed still settles into a steady value as $\delta \to \infty$. However, this time, the initial and terminal speeds depend on a non-trivial combination of the squirmer and/or droplet eccentricities and χ. For C_1 and $\chi = 1.05$ ($\chi = 1.5$), the squirmer's initial speed increases (decreases) with increasing e_s, as illustrated in Fig. 3(c). The absolute difference between speeds at both values of the eccentricity decreases with increasing χ. This dynamic is also observed in C_2 [Fig. 3(f)], where the combination of eccentricities $e_s = 0.3$ and $e_d = 0.9$ yields larger (smaller) initial speeds compared to $e_s = 0.9$ and $e_d = 0.3$ for $\chi = 1.5$ ($\chi = 2$). The last configuration C_3 shows insignificant variations between the speeds for a fixed χ and increasing e_d. The terminal speeds on the other end [Figs. 3(c), 3(f), and 3(i)] follow the same behavior as described for $\lambda \leq 1$.

While the above analysis described some of the differences observed from each configuration, taken as a whole, Fig. 3 reveals a number of common features. First, when $\delta < 1$, initial velocities of all configurations remain relatively constant, suggesting that sparse networks of stationary objects in the outer phase have a minimal impact on the squirmer's propulsion speed. However, as δ increases beyond 1, speeds decrease monotonically, converging to a steady value as $\delta \to \infty$. Second, U_S is independent of the fluid resistance, and the squirmer's and droplet's eccentricities as $\chi \to \infty$. In this case, the droplet enclosure no longer has any effects of the squirmer, which propels as if in an unbounded homogeneous domain ($U_S = U_N$). Third, for $\delta \to \infty$ and $\chi > 1$, the speed settles into a non-zero steady value, indicating that the squirmer is always able to move inside its cage, independently of the droplet's motion. In the case $\chi \approx 1$, the terminal speed $U_S = U_B$, the speed of an unbounded squirmer in a heterogeneous medium.[23]

For configurations C_1 and C_2, the droplet speed U_D is always positive and approaches zero as the fluid resistance increases. In other words, the droplet can no longer propel at very large values of the fluid resistance. However, we observe a novel behavior for C_3. While the droplet ultimately comes to a standstill as $\delta \to \infty$, there is a finite

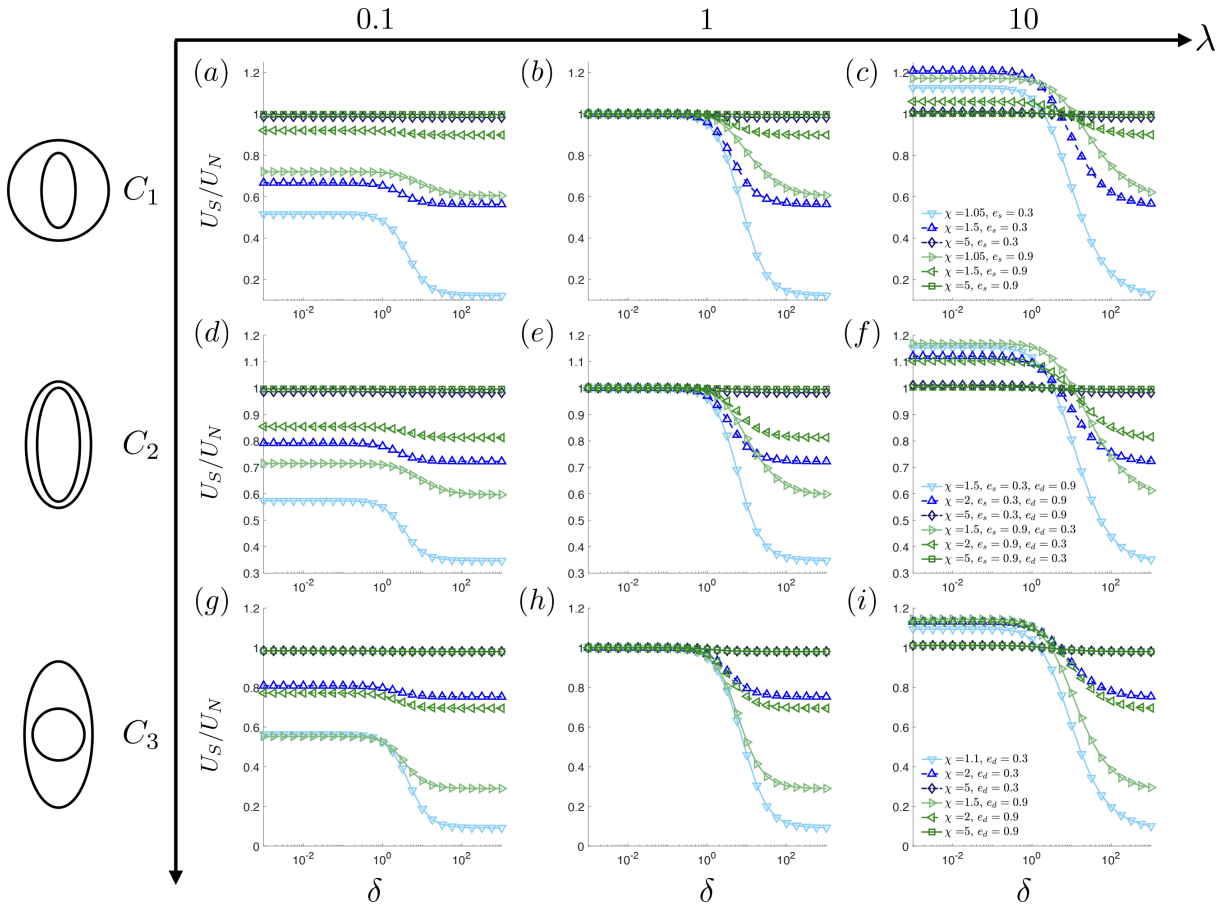

FIG. 3. Propulsion speed of the squirmer (vertical axes) as a function of the fluid resistance [horizontal axe: (a)–(c)]: spheroidal squirmer in a spherical droplet ($e_d = 0$); (d)–(f): spheroidal squirmer in a spheroidal droplet; and (g)–(i): spherical squirmer ($e_s = 0$) in a spheroidal droplet. The viscosity ratio varies from $\lambda = 0.1$ [first column: (a), (d), (g)] to $\lambda = 1$ [second column: (b), (e), (h)] and $\lambda = 10$ [third column: (c), (f), (i)]. The speed is scaled by $U_N = \tau_0[\tau_0 - (\tau_0^2 - 1)\coth^{-1}\tau_0]$ (a)–(f) or $U_N = 2/3$ (g)–(i), the propulsion speed of a spheroidal/spherical squirmer in an unbounded Newtonian fluid. For each configuration, the curves are color-coded as indicated in the legend in panels [(c), (f), (i)].

range of fluid resistance where $U_D < 0$, indicating a backward motion of the droplet.

Figure 4 shows the ratio U_D/U_S for configurations C_1 (a), C_2 (b), and C_3 (c) with $\lambda = 1$. Since the squirmer always propels forward ($U_S > 0$, Fig. 3), the change in sign in Fig. 4(c) implies $U_D < 0$. This backward motion only appears for small values of χ (in our simulations, $\chi = 1.1$ for $e_d = 0.3$ or $\chi = 1.5$ for $e_d = 0.9$). Moreover, the range and extent to which the droplet propels backward show a strong dependence on the viscosity ratio. For $\lambda \leq 10$, the range gets wider as $\lambda \to 0$. This widening range is illustrated in Fig. 4(d), where the backward motion dominates for $\delta \geq 31.6228$ at $\lambda = 0.1$ compared with $\delta \geq 177.8279$ at $\lambda = 10$. While $|U_D/U_S|$ gets smaller as λ nears 10, the backward motion actually becomes more pronounced for $\lambda \gg 10$ (at $\delta = 10^3$, $|U_D/U_S| \approx 0.2$ for $\lambda = 10^3$ compared with $|U_D/U_S| \approx 0.05$ for $\lambda = 10$). The droplet's backward motion can be explained, at least partially, by comparing the flow field and surface velocities for $U_D/U_S > 0$ vs $U_D/U_S < 0$.

Figure 5(a) shows the flow field for $U_D/U_S > 0$ (left half, $\delta \approx 17.8$) and $U_D/U_S < 0$ (right half, $\delta \approx 31.6$) for $\lambda = 0.1$, $\chi = 1.1$, and $e_d = 0.3$ In the droplet's forward motion, the flow field resembles that of an unbounded squirmer and the droplet is entrained along with the squirmer. In this case, the surface velocities on the squirmer and droplet point in the swimming direction, as illustrated in the left half of Fig. 5(b). By contrast, the backward motion of the droplet is characterized by vortex-like patterns that push (pull) at the front (and back) of the droplet. The surface velocities on the right half of Fig. 5(b) also confirm this opposite motion, with the squirmer propelling forward (red arrows) while the droplet is moving backward (blue arrows).

In conclusion, we investigated the combined effects of heterogeneity and shape on squirming with a cage. In terms of designing a drug delivery system, our results have important implications that we now discuss. We posit that two objectives must be achieved: drug dosage/content and speed of delivery.

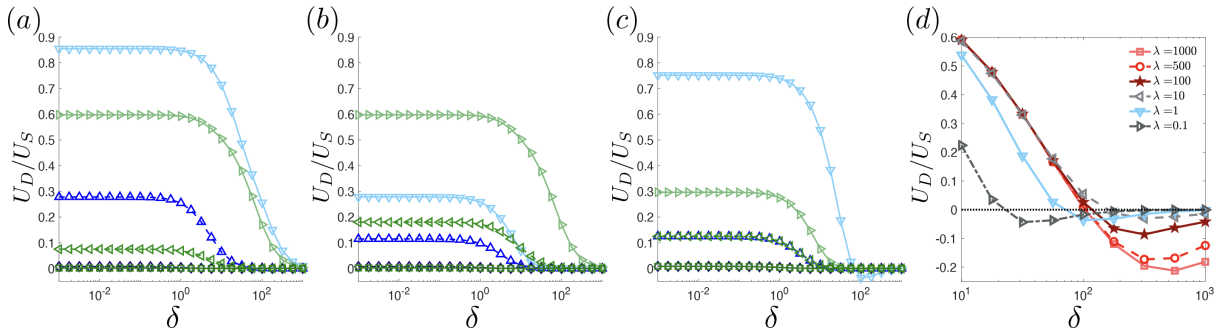

FIG. 4. Ratios of (a) the spherical droplet ($e_d = 0$) speed to the spheroidal squirmer speed, (b) the spheroidal droplet speed to the spheroidal squirmer speed, and (c) the spheroidal droplet speed to the spherical squirmer ($e_s = 0$) speed as a function of the fluid resistance with $\lambda = 1$. Panels in (a)–(c) are color-coded to correspond to the squirmer's speeds in Figs. 3(b), 3(e), and 3(h). In (d), the ratio is plotted for the spherical squirmer ($e_s = 0$) in a spheroidal droplet ($e_d = 0.3$). The panel shows changes in the range of fluid resistance and magnitude of the ratio that correspond to the backward propelling droplet ($U_D/U_S < 0$). Each curve represents different values of the viscosity ratio λ.

In any of the three geometries considered, the highest value of χ shows almost a complete resistance to any change in velocity as hydrodynamic resistance δ increases. These results suggest that a distribution pathway that experiences significant variations in δ, or alternatively is densely populated throughout, is best suited for configurations with high χ values. Additionally, the volume of drug contained in each droplet is directly proportional to χ, and subsequently must also be considered to ensure an ideal drug dosage. In cases where the distribution pathway is identified as being relatively sparse ($\delta < 1$), it may be possible to adjust the viscosity of the inner phase to increase the value of λ. In this hypothetical situation, a decreased χ value could result in enhanced propulsion speeds of the delivery system to the target site, thereby enabling timely treatment. Therefore, fully understanding both the distribution pathway and the required therapeutic dosage is critical for determining parameter values that maximize the effectiveness of a squirmer/droplet targeted therapy.

For its part, the backward motion of the droplet provides a decelerating mechanism, whereas the carrier's motion is reversed as opposed to suppressed by large fluid resistance. Note that this behavior is not a purely theoretical possibility, considering that the fluid resistance δ for a micro-sized squirmer[23] is estimated to be between 0.6 and 25. The upper limit falls well within the range where the backward droplet motion would begin occuring ($17.8 < \delta < 31.6$ for $\lambda = 0.1$). In experiments, the distinct flow patterns can be observed using Particle Image Velocimetry (PIV), which would help differentiate and/or identify carriers dynamics. The experimental data, coupled with theoretical analysis, would in turn aid to predict the interaction between the squirmer-droplet system and highly heterogeneous biological barriers.[6]

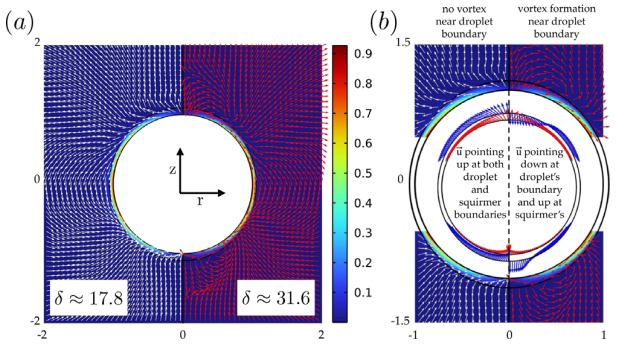

FIG. 5. (a) Flow field for the spherical squirmer ($e_s = 0$) in spheroidal droplet ($e_d = 0.3$) with $\lambda = 0.1$, $\chi = 1.1$, and $\delta \approx 17.8$ (left half; the squirmer and droplet propel forward along the positive z direction) or $\delta \approx 31.6$ (right half; the squirmer propels forward while the droplet moves backward). (b) Zooming into panel (a) to magnify the flow field near the squirmer-droplet system. The corresponding surface velocities or the squirmer (red arrows) and droplet (blue arrows) are shown on the graphic at the center of the squirmer. The color bar shows the magnitude of the velocity field.

Knowledge from our results is useful in guiding the choice of design parameters for effective drug carriers. It provides several considerations that may be tailored to specific objectives. However, we note that other considerations exist that have not been discussed. For example, the efficiency of the squirmer could be leveraged in determining the optimal combination of droplet size and squirming speed. Higher modes of swimming gait, critical for propulsion in complex fluids,[20,51] could also be considered. Moreover, determining how optimal propulsion strategies in unbounded domains[52–55] may change when the squirmers are encapsulated inside the droplets presents yet another line of inquiry. Future work in these directions is under way.

J.D.-G. and H.N. gratefully acknowledge funding support from the National Science Foundation Grant No. 2211633. H.N. also acknowledges support from a Jess and Mildred Fisher Endowed Professor of Mathematics from the Fisher College of Science and Mathematics at Towson University.

AUTHOR DECLARATIONS

Conflict of Interest

The authors have no conflicts to disclose.

Author Contributions

James Della-Giustina: Formal analysis (equal); Validation (equal); Visualization (equal); Writing – review & editing (equal). **Herve Nganguia:** Conceptualization (lead); Formal analysis (equal); Funding acquisition (lead); Methodology (equal); Project administration

(equal); Supervision (lead); Validation (equal); Visualization (equal); Writing – original draft (lead); Writing – review & editing (equal). **Ebru Demir:** Data curation (lead); Formal analysis (equal); Methodology (equal); Project administration (equal); Software (lead); Validation (equal); Visualization (equal); Writing – review & editing (equal).

DATA AVAILABILITY

The data that support the findings of this study are available from the corresponding authors upon reasonable request.

REFERENCES

[1]D. Samanta, N. Hosseini-Nassab, and R. N. Zare, "Electroresponsive nanoparticles for drug delivery on demand," Nanoscale **8**, 9310 (2016).
[2]J. Kolosnjaj-Tabi, L. Gibot, I. Fourquaux, M. Golzio, and M.-P. Rols, "Electric field-responsive nanoparticles and electric fields: Physical, chemical, biological mechanisms and therapeutic prospects," Adv. Drug Delivery Rev. **138**, 56–67 (2019).
[3]W. Wei, J. Sung, X.-Y. Guo, X. Chen, R. Wang, C. Qiu, H.-T. Zhang, W.-H. Pang, J.-C. Wang, and Q. Zhang, "Microfluidic-based holonomic constraints of siRNA in the kernel of lipid/polymer hybrid nanoassemblies for improving stable and safe in vivo delivery," ACS Appl. Mater. Interfaces **12**, 14839–14854 (2020).
[4]D. Chang, Y. Ma, X. Xu, J. Xie, and S. Ju, "Stimuli-responsive polymeric nanoplatforms for cancer therapy," Front. Bioeng. Biotechnol. **9**, 707319 (2021).
[5]J. A. Kemp and Y. J. Kwon, "Cancer nanotechnology: Current status and perspectives," Nano Convergence **8**, 34 (2021).
[6]H. Zhang, Z. Li, C. Gao, X. Fan, Y. Pang, T. Li, Z. Wu, H. Xie, and Q. He, "Dual-responsive bio hybrid neutrobots for active target delivery," Sci. Rob. **6**, eaaz9519 (2021).
[7]A. Fabozzi, F. Della Sala, M. di Gennaro, M. Barretta, G. Longobardo, N. Solimando, M. Pagliuca, and A. Borzacchiello, "Design of functional nanoparticles by microfluidic platforms as advanced drug delivery systems for cancer therapy," Lab Chip **23**, 1389 (2023).
[8]Y. Liu, J. Tan, A. Thomas, D. Ou-Yang, and V. R. Muzykantov, "The shape of things to come: Importance of design in nanotechnology for drug delivery," Ther. Delivery **3**, 181–194 (2012).
[9]S. Nejati, E. M. Vadeghani, S. Khorshidi, and A. Karkhaneh, "Role of particle shape on efficient and organ-based drug delivery," Eur. Polym. J. **122**, 109353 (2020).
[10]M. Cooley, A. Strode, M. Hoore, D. A. Fedosov, S. Mitragotri, and A. S. Gupta, "Influence of particle size and shape on their margination and wall-adhesion: Implications in drug delivery vehicle design across nano-to-micro scale," Nanoscale **10**, 15350–15364 (2018).
[11]M. J. Mitchell, M. M. Billingsley, R. M. Haley, M. E. Wechsler, N. A. Peppas, and R. Langer, "Engineering precision nanoparticles for drug delivery," Nat. Rev. Drug Discovery **20**, 101–124 (2021).
[12]Z. Wu, Y. Chen, D. Mukasa, O. S. Pak, and W. Gao, "Medical micro/nanorobots in complex media," Chem. Soc. Rev. **49**, 8088–8112 (2020).
[13]G. I. Taylor, "Analysis of the swimming of microscopic organisms," Proc. R. Soc. London, Ser. A **209**, 447–461 (1951).
[14]M. J. Lighthill, "On the squirming motion of nearly spherical deformable bodies through liquids at very small Reynolds numbers," Commun. Pure Appl. Math. **5**, 109–118 (1952).
[15]T. S. Yu, E. Lauga, and A. E. Hosoi, "Experimental investigations of elastic tail propulsion at low Reynolds number," Phys. Fluids **18**, 091701 (2006).
[16]E. Lauga, "Propulsion in a viscoelastic fluid," Phys. Fluids **19**, 083104 (2007).
[17]A. M. Leshansky, "Enhanced low-Reynolds number propulsion in heterogeneous viscous environments," Phys. Rev. E **80**, 051911 (2009).
[18]L. Zhu, M. Do-Quang, E. Lauga, and L. Brandt, "Locomotion by tangential deformation in a polymeric fluid," Phys. Rev. E **83**, 011901 (2011).
[19]O. S. Pak, L. Zhu, L. Brandt, and E. Lauga, "Micropropulsion and microrheology in complex fluids via symmetry breaking," Phys. Fluids **24**, 103102 (2012).
[20]C. Datt, L. Zhu, G. J. Elfring, and O. S. Pak, "Squirming through shear-thinning fluids," J. Fluid Mech. **784**, R1 (2015).
[21]E. Lauga, "Bacterial hydrodynamics," Annu. Rev. Fluid Mech. **48**, 105–130 (2016).
[22]S. Gómez, F. A. Godínez, E. Lauga, and R. Zenit, "Helical propulsion in shear-thinning fluids," J. Fluid Mech. **812**, R3 (2017).
[23]H. Nganguia and O. S. Pak, "Squirming motion in a brinkman medium," J. Fluid Mech. **855**, 554–573 (2018).
[24]J. H. Lee and Y. Yeo, "Controlled drug release from pharmaceutical nanocarriers," Chem. Eng. Sci. **125**, 75–84 (2015).
[25]M. R. Raveshi, M. S. A. Halim, S. N. Agnihotri, M. K. O'Bryan, A. Neild, and R. Nosrati, "Curvature in the reproductive tract alters sperm-surface interactions," Nat. Commun. **12**, 3446 (2021).
[26]J. Clausal-Tormos, D. Lieber, J.-C. Baret, A. El-Harrak, O. J. Miller, L. Frenz, J. Blouwolff, K. J. Humphry, S. Köster, H. Duan, C. Holtze, D. A. Weitz, A. D. Griffiths, and C. A. Merten, "Droplet-based microfluidic platforms for the encapsulation and screening of mammalian cells and multicellular organisms," Chem. Biol. **15**, 427–437 (2008).
[27]H. Wen, Y. Yu, G. Zhu, L. Jang, and J. Qin, "A droplet microchip with substance exchange capability for the developmental study of *C. elegans*," Lab Chip **15**, 1905–1911 (2015).
[28]Y. Ding, F. Qiu, X. C. Solvas, F. W. Y. Chiu, B. J. Nelson, and A. DeMello, "Microfluidic-based droplet and cell manipulations using artificial bacterial flagella," Micromachines **7**, 25 (2016).
[29]S. A. Mirbagheri and H. C. Fu, "*Helicobacter pylori* couples motility and diffusion to actively create a heterogeneous complex medium in gastric mucus," Phys. Rev. Lett. **116**, 198101 (2016).
[30]S. Y. Reigh and E. Lauga, "Two-fluid model for locomotion under self-confinement," Phys. Rev. Fluids **2**, 093101 (2017).
[31]S. Y. Reigh, L. Zhu, F. Gallaire, and E. Lauga, "Swimming with a cage: Low-Reynolds-number locomotion inside a droplet," Soft Matter **13**, 3161 (2017).
[32]A. Daddi-Moussa-Ider, H. Lowen, and S. Gekle, "Creeping motion of a solid particle inside a spherical elastic cavity," Eur. Phys. J. E **41**, 104 (2018).
[33]C. Hoell, H. Lowen, A. M. Menzel, and A. Daddi-Moussa-Ider, "Creeping motion of a solid particle inside a spherical elastic cavity: II. Asymmetric motion," Eur. Phys. J. E **42**, 89 (2019).
[34]H. Nganguia, L. Zhu, D. Palaniappan, and O. S. Pak, "Squirming in a viscous fluid enclosed by a Brinkman medium," Phys. Rev. E **101**, 063105 (2020).
[35]V. A. Shaik, V. Vasani, and A. M. Ardekani, "Locomotion inside a surfactant-laden drop at low surface Péclet numbers," J. Fluid Mech. **851**, 187–230 (2018).
[36]K. J. Marshall and J. F. Brady, "The hydrodynamics of an active squirming particle inside of a porous container," J. Fluid Mech. **919**, A31 (2021).
[37]J. Rutllant, M. Lopez-Bejar, and F. Lopez-Gatius, "Ultrastructural and rheological properties of bovine vaginal fluid and its relation to sperm motility fertilization: A Review," Reprod. Domest. Anim. **40**, 79–86 (2005).
[38]J. Radolf and S. Lukehart, *Pathogenic Treponema: Molecular and Cellular Biology* (Caister Academic Press, Norfolk, England, 2006).
[39]J. P. Celli, B. S. Turner, N. H. Afdhal, S. Keates, I. Ghiran, C. P. Kelly, R. H. Ewoldt, G. H. McKinley, P. So, S. Erramilli, and R. Bansil, "*Helicobacter pylori* moves through mucus by reducing mucin viscoelasticity," Proc. Natl. Acad. Sci. U. S. A. **106**, 14321–14326 (2009).
[40]C. W. Wolgemuth, "Flagellar motility of the pathogenic spirochetes," Semin. Cell Dev. Biol. **46**, 104–112 (2015).
[41]H. C. Brinkman, "Calculation of the viscous force exerted by a flowing fluid on a dense swarm of particles," Appl. Sci. Res. **1**, 27–34 (1949).
[42]S. Jung, "*Caenorhabditis elegans* swimming in a saturated particulate system," Phys. Fluids **22**, 031903 (2010).
[43]K. Leiderman and S. D. Olson, "Swimming in a two-dimensional Brinkman fluid: Computational modeling and regularized solutions," Phys. Fluids **28**, 021902 (2016).
[44]M. Lisicki, M. F. V. Rodrigues, R. E. Goldstein, and E. Lauga, "Swimming eukaryotic microorganisms exhibit a universal speed distribution," eLife **8**, e44907 (2019).
[45]M. F. V. Rodrigues, M. Lisicki, and E. Lauga, "The bank of swimming organisms at the micron scale (BOSO-Micro)," PLoS One **16**, e0252291 (2021).

[46]S. R. Keller and T. Y. Wu, "A porous prolate-spheroidal model for ciliated micro-organisms," J. Fluid Mech. **80**, 259–278 (1977).
[47]K. Ishimoto and E. A. Gaffney, "Swimming efficiency of spherical squirmers: Beyond the Lighthill theory," Phys. Rev. E **90**, 012704 (2014).
[48]M. Theers, E. Westphal, G. Gompper, and R. G. Winkler, "Modeling a spheroidal microswimmer and cooperative swimming in a narrow slit," Soft Matter **12**, 7372 (2016).
[49]R. Pohnl, M. N. Popescu, and W. E. Uspal, "Axisymmetric spheroidal squirmers and self-diffusiophoretic particles," J. Phys.: Condens. Matter **32**, 164001 (2020).
[50]J. R. Blake, "A spherical envelope approach to ciliary propulsion," J. Fluid Mech. **46**, 199–208 (1971).
[51]K. Pietrzyk, H. Nganguia, C. Datt, L. Zhu, G. J. Elfring, and O. S. Pak, "Flow around a squirmer in a shear-thinning fluid," J. Non-Newtonian Fluid Mech. **268**, 101–110 (2019).
[52]A. Vilfan, "Optimal shapes of surface slip driven self-propelled microswimmers," Phys. Rev. Lett. **109**, 128105 (2012).
[53]H. Guo, H. Zhu, R. Liu, M. Bonnet, and S. Veerapaneni, "Optimal slip velocities of micro-swimmers with arbitrary axisymmetric shapes," J. Fluid Mech. **910**, A26 (2021).
[54]A. Daddi-Moussa-Ider, B. Nasouri, A. Vilfan, and R. Golestanian, "Optimal swimmers can be pullers, pushers or neutral depending on the shape," J. Fluid Mech. **922**, R5 (2021).
[55]B. Nasouri, A. Vilfan, and R. Golestanian, "Minimum dissipation theorem for microswimmers," Phys. Rev. Lett. **126**, 034503 (2021).